

Quantum Bipolar Thermoelectricity

F. Antola^{1,*}, G. De Simoni^{1,†} and F. Giazotto^{1‡}
NEST Istituto Nanoscienze-CNR and Scuola Normale Superiore, I-56127 Pisa, Italy

A. Braggio^{1,2§}
*NEST Istituto Nanoscienze-CNR and Scuola Normale Superiore, I-56127 Pisa, Italy and
 Institute for Quantum Studies, Chapman University, Orange, CA 92866, USA*

Thermoelectricity usually originates from energy-dependent transport asymmetries. In this Letter, we explore a purely *quantum* thermoelectric effect rooted in the emission/absorption asymmetry of a low-temperature quantum bath. We propose a gap-asymmetric S-I-S' superconducting tunnel junction in thermal equilibrium, coupled to a low-temperature electromagnetic environment, which develops a nonlinear quantum bipolar thermoelectric effect due to the dynamical Coulomb blockade. Key performance features are analyzed for realistic implementations.

Introduction- A key question in quantum physics is how quantum fluctuations of the electromagnetic environment can induce complex electronic phenomena [1–4]. Although thermoelectricity is usually understood within a classical diffusive framework [5], it is natural to ask whether purely quantum features can also generate thermoelectric effects [6, 7]. This question has been investigated in quantum dots, where discrete energy levels enable energy filtering and thermoelectric conversion at the single-electron level [8–13]. Superconducting tunnel junctions, because of their sharp energy-dependent density of states (DOS), strongly enhance photon-assisted processes and are therefore highly sensitive to quantum fluctuations [14–17]. They have recently attracted attention as platforms for quantum thermal machines [18–21], as probes of electromagnetic environments [22–28] and for developing strong thermoelectric effects [29–32]. In this Letter, we introduce an entirely *quantum* mechanism for the generation of bipolar thermoelectricity within a superconducting tunnel junction with asymmetric energy gaps, where the junction is kept in thermal equilibrium but coupled to a cold electromagnetic environment.

Quantum thermoelectricity- In quantum transport, linear thermoelectric generation emerges from the breaking of the energy symmetry of electronic states around the Fermi energy E_F [6, 33]. Here, we show that a thermoelectric response can arise even in an ideally energy-symmetric system, driven by an imbalance between photon emission and absorption at energy $\hbar\omega$, when coupled to a cold reservoir with $k_B T \lesssim \hbar\omega$. [34] Such a quantum regime can be realized in an S-I-S' tunnel junction between superconductors with different gaps Δ and Δ' , where the relevant energy scale is $\hbar\omega \approx \Delta - \Delta'$ [35–37]. In these systems, the superconducting DOSs divergences enhance the weight of photon-assisted quasi-particle transitions, which dominates over the suppressed Josephson component [38, 39]. This suppression can be achieved via SQUID interferometry [32], tuning the Fraunhofer effect with an in-plane magnetic field [40], or with very opaque tunneling barriers with small Josephson energy [41].

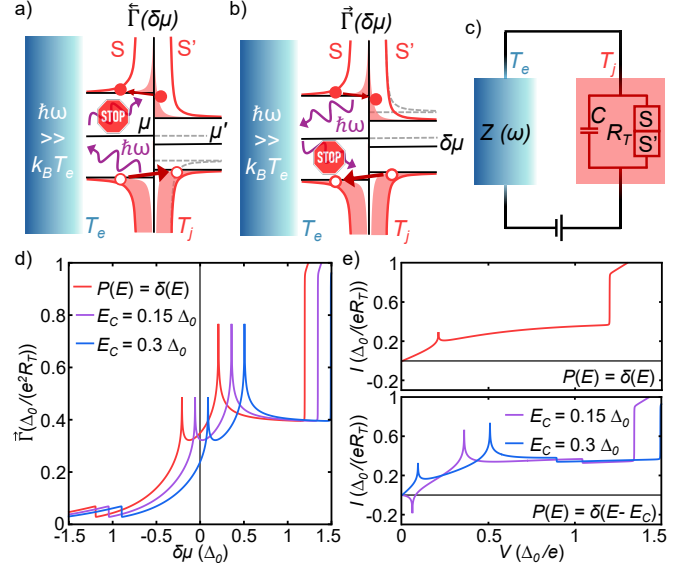


FIG. 1. (a) Quasiparticle occupation at temperature T_j for an S-I-S' junction biased at $\delta\mu$. The sketch illustrates backward tunneling processes $\tilde{\Gamma}(\delta\mu)$ enabled by photon-assisted transitions at $\hbar\omega$. Full (empty) red circles indicate particle (hole) excitations involved. The "STOP" sign denotes suppressed absorption due to the quantum nature of the environment at low T_e . Gray dashed lines represent the $\delta\mu = 0$ condition. (b) Same as in (a), but for the forward tunneling $\tilde{\Gamma}(\delta\mu)$. (c) Minimal circuit: an S-I-S' junction (capacitance C , tunnel resistance R_T) coupled to an environmental impedance $Z(\omega)$ and to an external bias. (d) Forward tunneling rate $\tilde{\Gamma}(\delta\mu)$ for two different charging energies E_C in the high-impedance (violet/blue) and low-impedance (red) regime. Other parameters: $\Delta'_0 = 0.9 \Delta_0$ and $T_j = 0.8 T_C$, where Δ_0 denotes the zero-temperature superconducting gap and T_C the critical temperature of the S electrode. (e) Corresponding current-voltage (I - V) characteristics.

Figures 1(a) and 1(b) schematically illustrate the backward $\tilde{\Gamma}(\delta\mu)$ and forward $\tilde{\Gamma}(\delta\mu)$ tunneling rates, respectively, for an asymmetric gap S-I-S' junction at temperature T_j and coupled to a cold environment at temperature T_e , with a slight bias $\delta\mu = \mu - \mu' > 0$. Both pro-

cesses are generally activated by the emission or absorption of an energy quanta around $\hbar\omega \approx \Delta - \Delta'$, with the corresponding particle (hole) states located at positive (negative) energies. When the environmental temperature satisfies $k_B T_e \lesssim \hbar\omega$, the system enters the quantum regime, where the bath can absorb but not emit energy (stop symbols in the picture). As a result, the asymmetry between emission and absorption selects predominantly hole (particle) processes for the backward (forward) rates. At zero bias ($\delta\mu = 0$, dashed gray lines), forward and backward tunneling rates coincide, yielding no net current: $I(\delta\mu) = e[\tilde{\Gamma}(\delta\mu) - \tilde{\Gamma}(\delta\mu)] = 0$. However, for finite bias $\delta\mu > 0$, the backward rate, dominated by hole processes, exceeds the forward one due to the monotonically decreasing DOS. A similar argument can be applied to the opposite case $\delta\mu < 0$. This mechanism induces a bipolar thermoelectric response that closely mirrors the conventional bipolar effect, despite the Fermi distributions in the leads being strictly identical and maintained at equilibrium [31, 32, 42]. Contrary to the conventional scenario, wherein the effect derives from a temperature difference across the junction, the present effect originates from the asymmetry in the radiative coupling between the S-I-S' junction and the surrounding cold electromagnetic environment. Moreover, the environment strongly affects transport *only* when the junction operates in the dynamical Coulomb blockade (DCB) regime, such as in the presence of a high-impedance environment [1, 43, 44].

Tunneling rates- We consider the circuit shown in Fig. 1(c), a tunnel junction of normal-state resistance R_T and intrinsic capacitance C , coupled via dissipationless wires to a remote external impedance $Z(\omega)$ that constitutes the electromagnetic environment. The total impedance seen by the junction is approximated as the parallel combination of its capacitance and the environmental impedance, $Z_t(\omega) = (i\omega C + Z^{-1}(\omega))^{-1}$. For a junction in thermal equilibrium at T_j and subject to a DC bias $\delta\mu = eV$, the forward tunneling rate $\tilde{\Gamma}(eV)$ reads [43]

$$\tilde{\Gamma}(eV) = \frac{1}{e^2 R_T} \int_{-\infty}^{\infty} dE dE' N_S(E) N_{S'}(E' + eV) \times f(E) [1 - f(E' + eV)] P(E - E'), \quad (1)$$

where $f(E) = 1/(1 + e^{E/k_B T_j})$ is the Fermi-Dirac distribution. The functions $N_i(E) = \left| \Re \left[\frac{E + i\gamma}{\sqrt{(E + i\gamma)^2 - \Delta_i^2(T_j)}} \right] \right|$ with $i = S, S'$ denote the normalized superconducting densities of states (DOSs) of the i th electrode with a temperature-dependent gap $\Delta_i(T_j)$, smeared by a nonzero Dynes parameter γ [35]. Fermi's golden rule rates contain a double integral due to the energy exchange $\Delta E = E - E'$ with the electromagnetic environment. This exchange is described by the function $P(\Delta E)$, which gives the probability that a tunneling event in-

volves an energy transfer ΔE to or from the environment. Positive (negative) values of ΔE correspond to energy emission (absorption). The function is defined as $P(\Delta E) = \frac{1}{2\pi\hbar} \int_{-\infty}^{\infty} dt e^{J(t) + \frac{i}{\hbar} \Delta E t}$, where the correlation function $J(t) = \langle [\tilde{\phi}(t) - \tilde{\phi}(0)] \tilde{\phi}(0) \rangle$ involves the phase operator $\tilde{\phi}(t) = \phi(t) - (e/\hbar) V t$ [43, 44]. The function $J(t)$ describes the influence of the electromagnetic environment and explicitly depends on its impedance $Z_t(\omega)$ (see the Supplementary Material [45]). For an impedance much smaller than the von Klitzing constant $R_K = h/e^2$, $\Re[Z_t(\omega)] \ll R_K$, the correlation function $J(t)$ vanishes and $P(E) \approx \delta(E)$, recovering the standard elastic tunneling rate with a single-energy integral [31, 35]. In the opposite regime of a strongly dissipative environment, $\Re[Z_t(\omega)] \approx R \gg R_K$, inelastic processes dominate, leading to the physics of the DCB [1, 43–45].

When the system and the environment are at the same temperature, $T_j = T_e = T$, the tunneling rates satisfy the detailed balance $\tilde{\Gamma}(-E) = e^{-\beta E} \tilde{\Gamma}(E)$, with $\beta = 1/k_B T$. This relation is also reflected in the function $P(\Delta E)$, with $P(-\Delta E) = e^{-\beta \Delta E} P(\Delta E)$ [43]. For symmetric DOS around the Fermi level, $N_i(E - E_F) = N_i(-(E - E_F))$, the current obeys the reciprocity relation $I(-V) = -I(V)$. In this regime of global thermal equilibrium, it reduces to $I(V) = e \tilde{\Gamma}(eV) (1 - e^{\beta eV})$, implying that quasiparticle transport is always dissipative, i.e., $I(V)V > 0$, regardless of the nature of the electromagnetic environment and consistent with what has been reported before [31]. Furthermore, the general reciprocity property ensures that $I(V=0) = 0$, forbidding any linear thermoelectric effect. However, in the following, we show that a nonlinear bipolar thermoelectric current of intrinsic *quantum* nature can still be generated when the junction is in thermal equilibrium, provided the electromagnetic environment is sufficiently cold.

Dissipative environment- We begin by considering a purely resistive electromagnetic environment, modeled as a frequency-independent resistor, $Z(\omega) = R$. The natural scale is conventionally expressed by the dimensionless conductance parameter $g = R_K/R$. In the limit of low environmental impedance ($g \rightarrow \infty$) and zero bath temperatures ($T_e \rightarrow 0$) there are no environmental corrections and $P(\Delta E) = \delta(\Delta E)$, recovering the standard elastic S-I-S' tunneling process described by the "semiconductor" model [35]. In this case, the tunneling rate corresponds to the red line in Fig. 1(d) and is independent of the capacitance C . For $eV > 0$, the rate increases rapidly when the energy difference exceeds $eV = \Delta + \Delta'$, leading to Ohmic-like behavior at higher bias. Below this threshold, in the subgap region, quasiparticle transport is strongly suppressed. However, a pronounced peak appears at the matching energy $\delta\mu = eV = \Delta - \Delta'$, resulting from the alignment of the singularities in the DOSs of the two superconducting electrodes. A secondary peak emerges at $eV = -(\Delta - \Delta')$ as a conse-

quence of detailed balance [46]. In the opposite regime of high impedance ($g \rightarrow 0$), the total effective impedance reduces to $\Re[Z_t(\omega)] \approx (\pi/C)\delta(\omega)$, allowing an analytical evaluation of the function $P(\Delta E) = \delta(\Delta E - E_C)$, where $E_C = e^2/(2C)$ is the charging energy. In this zero-temperature limit, the environment will absorb at least this additional energy. The tunneling rate, see violet and blue lines in Fig. 1(d), becomes capacitance-dependent and retains the same shape as in the low-impedance case, but shifted by Coulomb energy E_C . This energy shift also indicates a disruption of thermal equilibrium as the detailed balance is violated due to the energy transfer with the cold environmental impedance. Furthermore, under the conditions specified in $E_C \lesssim \Delta - \Delta'$, the system can transition to a regime characterized by a "strong" violation of detailed balance [47], where $\Gamma(-eV) > \Gamma(eV)$. This phenomenon is clearly illustrated in Fig. 1(d) (violet line), signaling the emergence of the bipolar thermoelectric effect induced by coupling with the electromagnetic environment. The current, shown in Fig. 1(e), confirms the discussed scenario. In the low impedance limit ($g \rightarrow \infty$, top panel), the I - V characteristic is *only* dissipative, as expected for an S-I-S' junction at equilibrium temperature T_j . In contrast, for $g \rightarrow 0$, the system is sensitive to the cold reservoir, and a peak emerges at $eV_P = \Delta - \Delta' - E_C$, which becomes thermoelectric (violet) when the "strong" violation of the detailed balance condition is realized in the rate. In this regime, a bipolar thermoelectric effect appears, with negative conductance around V_P , even though the S-I-S' junction remains locally in thermal equilibrium. A nonlocal temperature difference between the junction and the colder environmental impedance is necessary, demonstrating the thermoelectric nature of the effect discussed. A key difference from the bipolar thermoelectric effect driven by a temperature difference across the junction [31, 32, 42] lies in the position of the matching peak, which is shifted toward zero by $e/2C$ due to the DCB Coulomb gap.[48] Importantly, the discussed effect does not originate from a nonequilibrium ratchet mechanism [49–51]. Indeed, increasing the asymmetry by taking the smaller gap $\Delta' \rightarrow 0$ causes the effect to disappear rather than grow. Moreover, the I - V characteristic remains fully reciprocal, excluding the simple diode effect [45]. Finally, we neglect Joule heating in the environmental resistor, assuming that it remains well thermalized with the cryostat.

Thermoelectric behavior- In Fig. 2(a) we show the maximal thermoelectric power, which is well approximated by the power value at the thermoelectric peak V_P , that is, $P_{\text{MAX}} \approx |I(V_P) \cdot V_P|$, as a function of E_C and T_j , for two values of the gap ratio $r = \Delta(0)'/\Delta(0)$. The power becomes appreciable only above a specific temperature T_j , as a sufficient number of quasiparticle/quasihole states in the small gap side is necessary to probe the emission/absorption asymmetry. The effect strengthens with increasing T_j and reaches optimal performance around

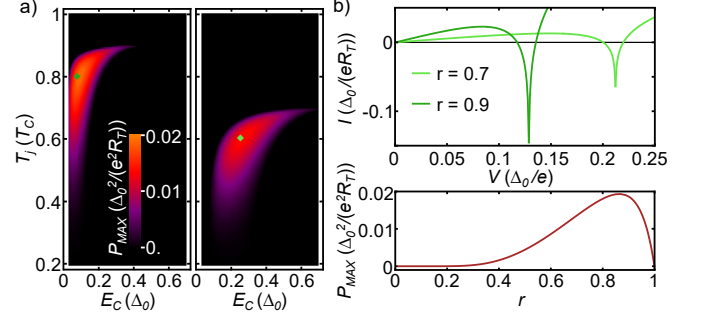


FIG. 2. (a) Thermoelectric power at the matching peak P_{MAX} as a function T_j and E_C , for $r = 0.9$ (left) and $r = 0.7$ (right). (b) Top panel: I - V characteristic under optimal conditions for $r = 0.9$ and $r = 0.7$. The parameters correspond to the stars shown in the respective color plots. Bottom panel: P_{MAX} computed at optimal E_C and T_j for different r .

$T_j \approx 0.9T'_C$, where T'_C is the critical temperature of the lower-gap electrode S' . In the results shown, the temperature dependence of the BCS self-consistent gaps causes both superconducting gaps to decrease with increasing temperature. However, their difference, $\Delta(T_j) - \Delta'(T_j)$, increases, allowing the emergence of quantum thermoelectricity at a higher level E_C , as shown in the picture. The upper panel of Fig. 2(b) shows the I - V characteristic at two optimal working points from Fig. 2(a), revealing enhanced power extraction and, correspondingly, a positive differential conductance near zero bias. The lower panel shows the extractable power as a function of the gap ratio r , evaluated at $T_j = 0.9T'_C$ with the Coulomb energy E_C set at its optimal value. As r increases, the power increases, peaks near $r \approx 0.9$, and then drops as the system approaches a symmetric S-I-S configuration. The disappearance of the thermoelectricity can also be interpreted as a transition to the classical limit, where symmetry between emission and absorption is restored, when $(\Delta - \Delta') \sim k_B T_e$.

Quantum regime- We now turn to the role of the environment temperature, which is directly linked to the *quantum* nature of the thermoelectric effect. To this end, we compute how the temperature of the electromagnetic environment affects quantum thermoelectricity. To model an experimentally realistic setup, we assume a finite value of g . In this case, we analytically compute $J(t)$ for the specific $Z_t(\omega)$ and obtain $P(\Delta E)$ by numerical Fourier integration [45]. Figure 3(a) shows the resulting I - V characteristic, demonstrating that thermoelectricity is strongly affected by environmental conditions. The peak at V_P broadens and decreases with increasing T_e as a consequence of the progressive reduction of the absorption/emission asymmetry in the environment at higher temperatures. The inset further confirms that also increasing g , reducing environmental impedance, suppresses the thermoelectric signal, due to the reduction of DCB physics. However, excessively in-

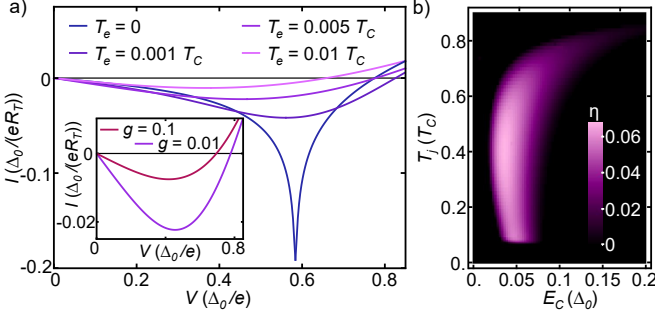


FIG. 3. (a) I - V characteristics for different values of T_e , with $g = 0.01$, $r = 0.9$, $E_C = 0.15\Delta_0$ and $T_j = 0.8T_C$. Inset: comparison between $g = 0.01$ and $g = 0.1$ at $T_e = 0.005T_C$. (b) Density plot of the efficiency η as a function of E_C and T_j , computed for $T_e = 0.005T_C$, $g = 0.01$ and $r = 0.9$.

creasing the environmental resistance value also reduces energy exchange between the junction and the reservoir due to the effects of impedance mismatch [52]. We therefore identify that the values of $g \approx 0.01$, corresponding to the resistance of a few M Ω are the most suitable. The discussed suppression of the peak can be phenomenologically described as a form of renormalization of the effective Dynes parameter Γ , which accounts for inelastic processes that effectively limit quasiparticle lifetime and smear the DOS. This is entirely consistent with the measured change in the Dynes parameter induced by modifications in the electromagnetic environment [53]. We estimate a maximum generated thermoelectric power of about 0.1 pW for a Nb/AlO_x/Nb junction with tunnel resistance $R_T \sim 100$ k Ω , gap ratio $r = 0.9$ and charging energy $E_C \sim 0.2$ mV, coupled to an environment with $R \sim 2.5$ M Ω and held at $T_e \sim 100$ mK. This results in a nonlinear Seebeck coefficient [52] of approximately 100 μ V/K, defined as $S = V_S/(T_j - T_e)$, where V_S is the bias voltage for which the current vanishes, $I(V_S) = 0$.

Thermoelectric efficiency- To further clarify the thermoelectric nature of the effect, it is essential to examine its thermodynamic efficiency. In this context, the two reservoirs are the hot junction and the cold electromagnetic environment. A meaningful definition of thermodynamic efficiency applies when the system operates as a power generator, that is, when $IV < 0$, and is given by the ratio of the useful electrical power to the total radiative energy transferred from the junction to the environment:

$$\eta = \frac{|I(V)V|}{\mathcal{P}_e(V)}. \quad (2)$$

The numerator is obtained directly from the current-voltage characteristic $I(V)$, while the denominator $\mathcal{P}_e(V)$ accounts for the heat flowing from the junction to the electromagnetic environment. The latter can be computed by generalizing the current expression to keep track of the energy flows instead of the charge [6], weighting the

integrand by the energy transferred into the environment ($E - E'$):

$$\begin{aligned} \mathcal{P}_e = \frac{1}{e^2 R_T} \int_{-\infty}^{\infty} dE dE' (E - E') N_S(E) N'_S(E' + eV) \\ f(E) [1 - f(E' + eV)] P(E - E') + \\ + (E' - E) N_S(E) N'_S(E' + eV) \\ [1 - f(E)] f(E' + eV) P(E' - E). \end{aligned} \quad (3)$$

This quantity satisfies the energy conservation in the junction, which yields

$$\dot{Q}(V) + \dot{Q}'(V) = I(V)V + \mathcal{P}_e(V), \quad (4)$$

where \dot{Q} and \dot{Q}' denote the heat currents flowing out of the two superconducting electrodes generalized within the $P(E)$ theory [20, 31, 45]. In Fig. 3(b), we show the behavior of η with respect to E_C and T_j , evaluated for the bias that maximizes thermopower extraction. As before, a nonlinear temperature dependence is observed. However, the efficiency remains appreciable even at extremely low temperatures. In particular, a minimum value of $T_j \approx 0.1T_C$ appears to be required to activate the process. The dependence E_C follows a trend similar to Fig. 2(a).

In the Supplementary Material [45], we discuss quantum thermoelectricity for a completely different quantum environment, where the impedance is purely inductive $Z(\omega) = i\omega L$, corresponding to a dissipationless resonant cavity at frequency $\omega_{LC} = 1/\sqrt{LC}$. We observe that this physics has similarity to the physics of the photon-assisted bipolar thermoelectric effect [54], which, however, completely disappears when the junction is at thermal equilibrium. Instead, in our case, the thermoelectricity persists even under junction equilibrium conditions, as it originates from the intrinsic emission-absorption asymmetry of the cold cavity.

Conclusion- We introduce a photonic-based bipolar quantum thermoelectric effect, which arises from the dynamical Coulomb blockade and the interaction of an electronic system with an electromagnetic environment within the quantum regime. The asymmetry between emission and absorption processes disrupts the intrinsic electron-hole symmetry, thereby allowing thermoelectricity to arise spontaneously even when the junction is locally in thermal equilibrium. We examined how the environmental resistive impedance and its temperature characterize the thermoelectric effect and its efficiency. Due to its quantum nature, the thermoelectric response exhibits a significant sensitivity to environmental temperature; however, the proposed mechanism can be scaled to higher temperatures by increasing the gap differences. These findings underscore the potential for non-equilibrium engineering of the electromagnetic environment in superconducting quantum technologies.

Acknowledgments- We acknowledge the EU Horizon 2020 Research and Innovation Framework Programme under Grant No. 101057977 (SPECTRUM) and the PNRR MUR project PE0000023-NQSTI for partial financial support. AB acknowledges also the MUR-PRIN2022 Project NETHQS (Grant No. 2022B9P8LN), the Royal Society through the International Exchanges between the UK and Italy (Grant No. IEC R2 192166), and the CNR Project QThER-MONANO. A.B. acknowledges the discussions with A. Jordan, B. Bhandari, A. N. Singh, F. Taddei, G. Marchegiani, and the hospitality provided by the Institute for Quantum Studies of Chapman University.

* filippo.antola@sns.it

† giorgio.desimoni@nano.cnr.it

‡ francesco.giazotto@sns.it

§ alessandro.braggio@nano.cnr.it

- [1] M. H. Devoret, D. Esteve, H. Grabert, G.-L. Ingold, H. Pothier, and C. Urbina, Effect of the electromagnetic environment on the Coulomb blockade in ultrasmall tunnel junctions, *Phys. Rev. Lett.* **64**, 1824 (1990).
- [2] T. Fujisawa, T. H. Oosterkamp, W. G. van der Wiel, B. W. Broer, R. Aguado, S. Tarucha, and L. P. Kouwenhoven, Spontaneous Emission Spectrum in Double Quantum Dot Devices, *Science* **282**, 932 (1998).
- [3] R. Aguado and L. P. Kouwenhoven, Double Quantum Dots as Detectors of High-Frequency Quantum Noise in Mesoscopic Conductors, *Phys. Rev. Lett.* **84**, 1986 (2000).
- [4] L. Henriët, A. N. Jordan, and K. Le Hur, Electrical current from quantum vacuum fluctuations in nanoengines, *Phys. Rev. B* **92**, 125306 (2015).
- [5] G. Grosso and G. P. Parravicini, *Solid State Physics* (Elsevier, 2000).
- [6] G. Benenti, G. Casati, K. Saito, and R. S. Whitney, Fundamental aspects of steady-state conversion of heat to work at the nanoscale, *Phys. Rep.* **694**, 1 (2017).
- [7] R. S. Whitney, Most Efficient Quantum Thermoelectric at Finite Power Output, *Phys. Rev. Lett.* **112**, 130601 (2014).
- [8] R. Sánchez and M. Büttiker, Optimal energy quanta to current conversion, *Phys. Rev. B* **83**, 085428 (2011).
- [9] G. Rosselló, R. López, and R. Sánchez, Dynamical Coulomb blockade of thermal transport, *Phys. Rev. B* **95**, 235404 (2017).
- [10] A. N. Jordan, B. Sothmann, R. Sánchez, and M. Büttiker, Powerful and efficient energy harvester with resonant-tunneling quantum dots, *Phys. Rev. B* **87**, 075312 (2013).
- [11] H. Thierschmann, R. Sánchez, B. Sothmann, F. Arnold, C. Heyn, W. Hansen, H. Buhmann, and L. W. Molenkamp, Three-terminal energy harvester with coupled quantum dots, *Nat. Nanotechnol.* **10**, 854 (2015).
- [12] M. Josefsson, A. Svilans, A. M. Burke, E. A. Hoffmann, S. Fahlvik, C. Thelander, M. Leijnse, and H. Linke, A quantum-dot heat engine operating close to the thermodynamic efficiency limits, *Nat. Nanotechnol.* **13**, 920 (2018).
- [13] G. Jaliel, R. Puddy, R. Sánchez, A. Jordan, B. Sothmann, I. Farrer, J. Griffiths, D. Ritchie, and C. Smith, Experimental Realization of a Quantum Dot Energy Harvester, *Phys. Rev. Lett.* **123**, 117701 (2019).
- [14] R. Deblock, E. Onac, L. Gurevich, and L. P. Kouwenhoven, Detection of Quantum Noise from an Electrically Driven Two-Level System, *Science* **301**, 203 (2003).
- [15] P.-M. Billangeon, F. Pierre, H. Bouchiat, and R. Deblock, Emission and Absorption Asymmetry in the Quantum Noise of a Josephson Junction, *Phys. Rev. Lett.* **96**, 136804 (2006).
- [16] J. Basset, H. Bouchiat, and R. Deblock, Emission and Absorption Quantum Noise Measurement with an On-Chip Resonant Circuit, *Phys. Rev. Lett.* **105**, 166801 (2010).
- [17] J. Basset, H. Bouchiat, and R. Deblock, High-frequency quantum admittance and noise measurement with an on-chip resonant circuit, *Phys. Rev. B* **85**, 085435 (2012).
- [18] J. P. Pekola and F. W. J. Hekking, Normal-Metal-Superconductor Tunnel Junction as a Brownian Refrigerator, *Phys. Rev. Lett.* **98**, 210604 (2007).
- [19] P. P. Hofer, J.-R. Souquet, and A. Clerk, Quantum heat engine based on photon-assisted Cooper pair tunneling, *Phys. Rev. B* **93**, 041418 (2016).
- [20] K. Y. Tan, M. Partanen, R. E. Lake, J. Govenius, S. Masuda, and M. Möttönen, Quantum-circuit refrigerator, *Nat. Commun.* **8**, 15189 (2017).
- [21] F. Antola, A. Braggio, G. De Simoni, and F. Giazotto, Tunable thermoelectric superconducting heat pipe and diode, *Supercond. Sci. Technol.* **37**, 115023 (2024).
- [22] J.-R. Souquet, M. J. Woolley, J. Gabelli, P. Simon, and A. A. Clerk, Photon-assisted tunnelling with nonclassical light, *Nat. Commun.* **5**, 5562 (2014).
- [23] N. Lörch, C. Bruder, N. Brunner, and P. P. Hofer, Optimal work extraction from quantum states by photo-assisted Cooper pair tunneling, *Quantum Sci. Technol.* **3**, 035014 (2018).
- [24] M. Mecklenburg, B. Kubala, and J. Ankerhold, Thermopower and dynamical Coulomb blockade in nonclassical environments, *Phys. Rev. B* **96**, 155405 (2017).
- [25] B. Karimi, D. Nikolić, T. Tuukkanen, J. T. Peltonen, W. Belzig, and J. P. Pekola, Optimized Proximity Thermometer for Ultrasensitive Detection, *Phys. Rev. Appl.* **13**, 054001 (2020).
- [26] D. Nikolić, B. Karimi, D. S. Rengel, J. P. Pekola, and W. Belzig, Optimized proximity thermometer for ultrasensitive detection: Role of an ohmic electromagnetic environment, *Phys. Rev. B* **108**, 024507 (2023).
- [27] S. Cailleaux, Q. Ficheux, N. Roch, and D. M. Basko, Theory of the Photonic Joule Effect in Superconducting Circuits, *Phys. Rev. Lett.* **134**, 227001 (2025).
- [28] M. Hübner, J. C. Cuevas, and W. Belzig, *Nonclassical Photon-Assisted Transport in Superconducting Tunnel Junctions* (2025), arXiv:2507.22662 [cond-mat].
- [29] P. Machon, M. Eschrig, and W. Belzig, Nonlocal Thermoelectric Effects and Nonlocal Onsager relations in a Three-Terminal Proximity-Coupled Superconductor-Ferromagnet Device, *Phys. Rev. Lett.* **110**, 047002 (2013).
- [30] F. S. Bergeret, M. Silaev, P. Virtanen, and T. T. Heikkilä, Colloquium: Nonequilibrium effects in superconductors with a spin-splitting field, *Rev. Mod. Phys.* **90**, 041001 (2018).
- [31] G. Marchegiani, A. Braggio, and F. Giazotto, Nonlinear Thermoelectricity with Electron-Hole Symmetric Sys-

- tems, *Phys. Rev. Lett.* **124**, 106801 (2020).
- [32] G. Germanese, F. Paolucci, G. Marchegiani, A. Braggio, and F. Giazotto, Bipolar thermoelectric Josephson engine, *Nat. Nanotechnol.* **17**, 1084 (2022).
- [33] L. Arrachea, A. Braggio, P. Burset, E. J. H. Lee, A. L. Yeyati, and R. Sánchez, *Thermoelectric processes of quantum normal-superconductor interfaces* (2025), arXiv:2507.22662 [cond-mat].
- [34] The reader should be aware that sometimes the energy symmetry is also imprecisely called particle-hole symmetry.
- [35] M. Tinkham, *Introduction to Superconductivity* (Courier Corporation, 2004).
- [36] S. Shapiro, P. H. Smith, J. Nicol, J. L. Miles, and P. F. Strong, Superconductivity and Electron Tunneling, *IBM J. Res. Dev.* **6**, 34 (1962).
- [37] P. Townsend and J. Sutton, Investigation by Electron Tunneling of the Superconducting Energy Gaps in Nb, Ta, Sn, and Pb, *Phys. Rev.* **128**, 591 (1962).
- [38] G. Marchegiani, A. Braggio, and F. Giazotto, Phase-tunable thermoelectricity in a Josephson junction, *Phys. Rev. Res.* **2**, 043091 (2020).
- [39] G. Germanese, F. Paolucci, G. Marchegiani, A. Braggio, and F. Giazotto, Phase Control of Bipolar Thermoelectricity in Josephson Tunnel Junctions, *Phys. Rev. Appl.* **19**, 014074 (2023).
- [40] J. M. Rowell, Magnetic Field Dependence of the Josephson Tunnel Current, *Phys. Rev. Lett.* **11**, 200 (1963).
- [41] M. Weides, Barriers in Josephson Junctions: An Overview, in *The Oxford Handbook of Small Superconductors*, edited by A. Narlikar (Oxford University Press, 2017) pp. 432–458.
- [42] G. Marchegiani, A. Braggio, and F. Giazotto, Superconducting nonlinear thermoelectric heat engine, *Phys. Rev. B* **101**, 214509 (2020).
- [43] G.-L. Ingold and Y. V. Nazarov, Charge Tunneling Rates in Ultrasmall Junctions, in *Single Charge Tunneling: Coulomb Blockade Phenomena In Nanostructures*, edited by H. Grabert and M. H. Devoret (Springer US, Boston, MA, 1992) pp. 21–107.
- [44] Y. V. Nazarov and Y. M. Blanter, *Quantum Transport: Introduction to Nanoscience* (Cambridge University Press, 2009).
- [45] See Supplemental Material at [URL will be inserted by publisher] for further details on the theoretical model and an additional example involving an environment with a single resonance frequency.
- [46] For $g \rightarrow \infty$, even if the electromagnetic environment is at different temperature, it practically does not affect the junction.
- [47] S. Battisti, G. De Simoni, L. Chirilli, A. Braggio, and F. Giazotto, Bipolar thermoelectric superconducting single-electron transistor, *Phys. Rev. Res.* **6**, L012022 (2024).
- [48] This phenomenology matches the charging effects reported over the bipolar thermoelectric effect of the single electron transistor [47].
- [49] H. Linke, T. E. Humphrey, A. Löfgren, A. O. Sushkov, R. Newbury, R. P. Taylor, and P. Omling, Experimental Tunneling Ratchets, *Science* **286**, 2314 (1999).
- [50] C. J. O. Reichhardt and C. Reichhardt, Ratchet Effects in Active Matter Systems, *Annu. Rev. Condens. Matter Phys.* **8**, 51 (2017).
- [51] J. P. Custer, J. D. Low, D. J. Hill, T. S. Teitsworth, J. D. Christesen, C. J. McKinney, J. R. McBride, M. A. Brooke, S. C. Warren, and J. F. Cahoon, Ratcheting quasi-ballistic electrons in silicon geometric diodes at room temperature, *Science* **368**, 177 (2020).
- [52] G. Marchegiani, A. Braggio, and F. Giazotto, Highly efficient phase-tunable photonic thermal diode, *Applied Physics Letters* **118**, 022602 (2021).
- [53] J. P. Pekola, V. F. Maisi, S. Kafanov, N. Chekurov, A. Kemppinen, Y. A. Pashkin, O.-P. Saira, M. Möttönen, and J. S. Tsai, Environment-Assisted Tunneling as an Origin of the Dynes Density of States, *Phys. Rev. Lett.* **105**, 026803 (2010).
- [54] A. Hijano, F. Bergeret, F. Giazotto, and A. Braggio, Microwave-Assisted Thermoelectricity in S-I-S' Tunnel Junctions, *Phys. Rev. Appl.* **19**, 044024 (2023).

Supplemental Material: Quantum Bipolar Thermoelectricity

F. Antola¹, G. De Simoni¹, F. Giazotto¹, A. Braggio^{1,2}

¹*NEST Istituto Nanoscienze-CNR and Scuola Normale Superiore, I-56127 Pisa, Italy*

²*Institute for Quantum Studies, Chapman University, Orange, CA 92866, USA*

THE $P(E)$ THEORY

In the main text, we express the tunneling rates for the superconducting junction [Eq. (1)] in terms of the $P(E)$ function, defined as:

$$P(\Delta E) = \frac{1}{2\pi\hbar} \int_{-\infty}^{\infty} dt e^{J(t) + \frac{i}{\hbar} \Delta E t}. \quad (\text{S1})$$

This corresponds to the Fourier transform of the exponential of the phase-phase correlation function, $J(t) = \langle [\tilde{\phi}(t) - \tilde{\phi}(0)] \tilde{\phi}(0) \rangle$, where $\tilde{\phi}(t) = \phi(t) - (e/\hbar)Vt$ denotes the phase fluctuations in the rotating frame defined by the voltage bias V [1,2]. The explicit expression for $J(t)$ is given by:

$$J(t) = 2 \int_0^{\infty} \frac{d\omega}{\omega} \frac{\text{Re}[Z_t(\omega)]}{R_k} \left\{ \coth \left(\frac{\beta_e \hbar \omega}{2} \right) [\cos(\omega t) - 1] - i \sin(\omega t) \right\}, \quad (\text{S2})$$

where $Z_t(\omega)$ is the effective environmental impedance seen by the SIS' junction. Note that phase fluctuations are strongly dependent on the inverse temperature of the electromagnetic environment $\beta_e = 1/(k_B T_e)$.

Purely Ohmic Environment

In this case, the total impedance takes the form $Z_t(\omega) = (i\omega C + 1/R)^{-1}$. It is convenient to consider the limit of a high-impedance (Ohmic) environment, where $\Re[Z_t(\omega)] \gg R_K$ ($g \rightarrow 0$). In this regime, the function can be expanded in the limit $\omega t \rightarrow 0$, yielding:

$$J(t) = -\frac{\pi}{R_k C} \left(\frac{1}{\hbar \beta} t^2 + it \right). \quad (\text{S3})$$

This leads to a Gaussian integral for $P(E)$:

$$P(E) = \frac{1}{\sqrt{4\pi E_C k_B T_e}} \exp \left[-\frac{(E - E_C)^2}{4E_C k_B T_e} \right], \quad (\text{S4})$$

which is a Gaussian centered at $E = E_C$, with variance $2E_C k_B T_e$. In the zero-temperature limit $T_e \rightarrow 0$, this expression reduces to $P(E) \rightarrow \delta(E - E_C)$, as discussed in the main text.

In the general case of an Ohmic environment with finite resistance, the phase correlation function reads:

$$J(t) = \frac{2}{g} \int_0^{\infty} \frac{d\omega}{\omega} \frac{1}{1 + (\omega/\omega_R)^2} \left\{ \coth \left(\frac{\hbar \omega}{2k_B T_B} \right) [\cos(\omega t) - 1] - i \sin(\omega t) \right\}, \quad (\text{S5})$$

where $\omega_R = 1/(RC)$ is the characteristic RC cutoff frequency. The imaginary and real parts can be computed separately using standard techniques from complex analysis. The imaginary part evaluates to:

$$\text{Im}[J(t)] = -\frac{\pi}{g} (1 - e^{-\omega_R t}). \quad (\text{S6})$$

The real part has a more involved structure and reads:

$$\text{Re}[J(t)] = -\frac{2\pi}{g} \left[\frac{t}{\hbar \beta} - \cot \left(\frac{\beta \hbar \omega_R}{2} \right) \frac{1 - e^{-\omega_R t}}{2} + \sum_{n=1}^{\infty} \frac{2}{\pi n} \frac{1}{1 - (2\pi n / (\beta \hbar \omega_R))^2} (1 - e^{-2\pi n t / \hbar \beta}) \right]. \quad (\text{S7})$$

Both expressions are consistent with the high-impedance limit $g \rightarrow 0$ given in Eq. S3.

FORWARD AND BACKWARD RATES

The forward (backward) tunneling rate corresponds to the transition probability that an electron of S (S') lead at energy E ($E' + eV$) tunnels into S' (S) at energy $E' + eV$ (E), by exchanging an energy $E - E'$ ($E' - E$) with the electromagnetic environment. This process is encoded in Eq. (1) of the main text. For completeness, we report here the expression for the backward rate:

$$\tilde{\Gamma}(eV) = \frac{1}{e^2 R_T} \int_{-\infty}^{\infty} dE dE' N_{S'}(E' + eV) N_S(E) f(E' + eV) [1 - f(E)] P(E' - E). \quad (\text{S8})$$

From the comparison of forward and backward rates, one finds that, for an energy-symmetric DOS, the two are related by the reciprocity relation.

$$\vec{\Gamma}(-eV) = \tilde{\Gamma}(eV). \quad (\text{S9})$$

This can be shown starting from Eq. (1) evaluated at $-eV$:

$$\begin{aligned} \vec{\Gamma}(-eV) &= \frac{1}{e^2 R_T} \int_{-\infty}^{\infty} dE dE' N_S(E) N_{S'}(E' - eV) f(E) [1 - f(E' - eV)] P(E - E') \\ &= \frac{1}{e^2 R_T} \int_{-\infty}^{\infty} dE dE' N_S(-E) N_{S'}(-E' - eV) f(-E) [1 - f(-E' - eV)] P(E' - E) \\ &= \frac{1}{e^2 R_T} \int_{-\infty}^{\infty} dE dE' N_S(E) N_{S'}(E' + eV) [1 - f(E)] f(E' + eV) P(E' - E) = \tilde{\Gamma}(eV), \end{aligned}$$

where in the second line we performed the change of variables $E \rightarrow -E$, $E' \rightarrow -E'$, and used the symmetry relations $N_i(-E) = N_i(E)$ and $f(-E) = 1 - f(E)$ for the DOSs and the Fermi function, respectively. We note that, although the reciprocity relation has been explicitly discussed for a junction in thermal equilibrium (as considered in this work), it can be shown to hold in general, even when the left and right leads are at different temperatures. Furthermore, the previous discussion shows that, due to the energy symmetry of the DOSs and of the Fermi function the rate reciprocal relation is still valid also when the junction is coupled with an electromagnetic environment kept at still another temperature T_e . Finally, the reciprocity relationship between the forward and backward rates directly implies the corresponding symmetry for the I - V characteristic. Since the current is given as $I(V) = e[\vec{\Gamma}(eV) - \tilde{\Gamma}(eV)]$, it immediately follows that

$$I(V) = -I(-V), \quad (\text{S10})$$

highlighting that if a thermoelectric effect is eventually found it must be bipolar and nonlinear in nature as discussed in the main text.

The reciprocity property, when the coupling to the environment described by the $P(\Delta E)$ function becomes significant, is directly related to the fact that voltage fluctuations across the junction *see* the electromagnetic environment as a linear element. This implies that the electromagnetic response is symmetric under the exchange $\delta V \rightarrow -\delta V$, meaning that the two sides of the junction are indistinguishable from the perspective of the environment. This symmetry is the fundamental reason why the observed thermoelectric effect is bipolar. Furthermore, it confirms that the effect cannot be explained as a simple rectification process, which would instead violate the reciprocity property, as discussed in the main text.

ENERGY BALANCE

To evaluate thermodynamic efficiency (see Eq. (2) of the main text), it is necessary to assess the heat exchanged, \mathcal{P}_e , between the hot reservoir (the junction) and the cold reservoir (the electromagnetic environment $Z(\omega)$). This quantity can be easily obtained by considering the energy conservation at the junction. In the thermoelectric regime, the total energy flow through the junction is split between the thermoelectrical power generated $-IV$ and the radiative power loss \mathcal{P}_e by the hot reservoir. The energy flow through the junction can easily be computed as the net heat exchanged during the tunneling process by examining the process from the two inequivalent superconducting leads of the junction. In particular, we define the heat currents \dot{Q} and \dot{Q}' , taken as positive when heat flows out of the S and

S' leads, respectively. The heat extracted from lead S is then

$$\begin{aligned} \dot{Q}(V) = \frac{1}{e^2 R_T} \int_{-\infty}^{\infty} dE dE' & EN_S(E) N_{S'}(E' + eV) f(E) [1 - f(E' + eV)] P(E - E') - \\ & - E' N_S(E) N_{S'}(E' + eV) [1 - f(E)] f(E' + eV) P(E' - E). \end{aligned} \quad (S11)$$

The corresponding heat extracted from lead S' is:

$$\begin{aligned} \dot{Q}'(V) = \frac{1}{e^2 R_T} \int_{-\infty}^{\infty} dE dE' & (-E - eV) N_S(E) N_{S'}(E' + eV) f(E) [1 - f(E' + eV)] P(E - E') + \\ & + (E' + eV) N_S(E) N_{S'}(E' + eV) [1 - f(E)] f(E' + eV) P(E' - E) \end{aligned} \quad (S12)$$

where we take the S lead to be grounded, i.e., $\mu_S = 0$. From the definition of current in the main text, the thermoelectric power generated by the junction is given by $-I(V)V$. Finally, to account for energy conservation, we must also consider the radiative energy exchanged with the electromagnetic environment. The corresponding radiative power lost by the junction can be easily computed by weighting the rate expression with ΔE , i.e., the argument of the $P(\Delta E)$ function, which represents the radiative energy flowed to the electromagnetic environment. Indeed, it becomes

$$\begin{aligned} \mathcal{P}_{env}(V) = \frac{1}{e^2 R_T} \int_{-\infty}^{\infty} dE dE' & (E - E') N_S(E) N_{S'}(E' + eV) f(E) [1 - f(E' + eV)] P(E - E') + \\ & + (E' - E) N_S(E) N_{S'}(E' + eV) [1 - f(E)] f(E' + eV) P(E' - E). \end{aligned} \quad (S13)$$

Is it possible to verify that the energy conservation in the tunnel junction (first principle)

$$\dot{Q}(V) + \dot{Q}'(V) = -I(V)V + \mathcal{P}_e(V) \quad (S14)$$

it is satisfied for each value of V independently if the electrical power is dissipated or produced at the junction.

ABSENCE OF THERMOELECTRICITY IN A NIS JUNCTION

The charge current in a normal metal–insulator–superconductor (NIS) junction is given by:

$$\begin{aligned} I(V) = \frac{1}{e R_T} \int_{-\infty}^{\infty} dE dE' & N(E) N_0 f(E) [1 - f(E' + eV)] P(E - E') \\ & - N(E) N_0 [1 - f(E)] f(E' + eV) P(E' - E), \end{aligned}$$

where N_0 is the constant density of states of the metallic island. We now perform the change of variables $E \rightarrow -E$, $E' \rightarrow -E'$ in the second term. The full current can thus be written as:

$$I(V) = \frac{1}{e R_T} \int_{-\infty}^{\infty} dE dE' N(E) N_0 f(E) P(E - E') [f(E' - eV) - f(E' + eV)].$$

We now observe that for $V > 0$, the difference

$$f(E' - eV) - f(E' + eV) \quad (S15)$$

is strictly positive for all E' , since the Fermi function decreases monotonically. Therefore, the integrand is everywhere non-negative and so $I(V) > 0$ for all $V > 0$, which implies that electrical power $I(V)V > 0$. This indicates that the system is always dissipative and cannot exhibit thermoelectric behavior.

QUANTUM BIPOLAR THERMOELECTRICITY FOR SINGLE-MODE ENVIRONMENT

As a different example, we can consider a system coupled to an environment with a single resonant frequency ω_{LC} , modeled in Fig. 1(a) by a pure inductance L in the impedance branch. The resulting total impedance has real part

$\text{Re}[Z_t(\omega)] = \frac{\pi}{2C} [\delta(\omega - \omega_{LC}) + \delta(\omega + \omega_{LC})]$, with $\omega_{LC} = 1/\sqrt{LC}$. The presence of the Dirac delta allows the integral in Eq. S2 to be analytically evaluated, yielding:

$$J(t) = \rho \left\{ \coth \left(\frac{1}{2} \beta \hbar \omega_{LC} \right) [\cos(\omega_{LC} t) - 1] - i \sin(\omega_{LC} t) \right\}. \quad (\text{S16})$$

This expression can be inserted into Eq. (2) of the main text to obtain [1]

$$P(E) = \exp \left[-\rho \coth \left(\frac{\beta \hbar \omega_{LC}}{2} \right) \right] \sum_{k=-\infty}^{+\infty} I_k \left(\frac{\rho}{\sinh \left(\frac{\beta \hbar \omega_{LC}}{2} \right)} \right) \exp \left(k \frac{\beta \hbar \omega_{LC}}{2} \right) \delta(E - k \hbar \omega_{LC}), \quad (\text{S17})$$

where I_k is the modified Bessel function of the first kind. In the zero-temperature limit $T_e \rightarrow 0$, this expression reduces to a Poisson series of discrete energy emissions:

$$P(E) = \sum_{k=0}^{+\infty} p_k \delta(E - k \hbar \omega_{LC}), \quad p_k = e^{-\rho} \frac{\rho^k}{k!}, \quad (\text{S18})$$

which describes the probability p_k of absorbing k quanta of energy from the environment. The dimensionless coupling $\rho = E_C/\hbar\omega_{LC}$ sets both the average number of emitted quanta and the width of the distribution.

Figure 4(a) shows the tunneling rates for an environment described by Eq. S18, with fixed $\rho = 0.2$ and varying ω_{LC} . We observe satellite peaks next to the matching peaks in the forward rate, located at $E = \pm(\Delta - \Delta') + \hbar\omega_{LC}$. For low values of ρ , only the first satellite peak is visible, since the multiphoton processes are strongly suppressed, consistent with the mentioned Poissonian statistics.

Unlike microwave-driven setups, where symmetric sidebands develop almost symmetrically around the main peaks [3], the low temperature of the cold bath $k_B T_e \ll \hbar\omega_{LC}$ (quantum regime) of the environment inhibits the emission process from the bath, yielding satellites only at higher energies. For photon-assisted processes induced by an active driving, where an infinite number of photons are available, absorption/emission processes are necessarily symmetric. This means that bipolar thermoelectricity can be *only* generated if a temperature difference is applied between the two terminals of the junction [3], while in thermal equilibrium the classical photon-assisted current can be only dissipative. Therefore, for a junction in thermal equilibrium, as considered in this paper, bipolar thermoelectricity can be *only* generated if the electromagnetic environment operates as a cold quantum bath. This highlights the purely *quantum* nature of the thermoelectric effect discussed in this work, in sharp contrast to previously reported mechanisms [4].

From the forward rates in the lower panel of Fig. 4(a), we observe that increasing ρ from small values enhances the satellite peaks' while progressively suppressing the primary matching peak. For specific values of the parameters, this may lead to a strong detailed balance violation $\bar{\Gamma}(-E) > \bar{\Gamma}(E)$ (see main text) and the onset of a thermoelectric regime, as in the resistive case. Higher-order processes involving multiple quanta may also become potentially accessible with sufficiently strong values of ρ . This results in additional satellite peaks, which may even develop other thermoelectric peaks with increasingly complex behavior.

Figure 4(b) shows the I - V characteristics for this single-mode environment. In particular, we see that the environment temperature T_e weakly affects the thermoelectric behavior, indicating greater robustness to thermal broadening compared to the purely resistive case discussed in the main text. As shown in the inset, the maximum T_e compatible with a detectable thermoelectric response depends on the resonance frequency: increasing the ω_{LC} frequency substantially reduces the required thermal difference, until the effect abruptly vanishes.

Figure 4(c) shows the extractable power from the first satellite peak P_{MAX} as a function of T_j and $\hbar\omega_{LC}$, in the regime $k_B T_e \ll \hbar\omega_{LC}$. The behavior mirrors Fig. 2(a): power increases with T_j , peaking near $0.9T'_C$. Here, $\hbar\omega_{LC}$ sets the position of the satellite and plays a role analogous to E_C in the resistive case, the optimal range shifting to higher frequencies as the temperature increases. Notably, power vanishes along a curve where a second satellite appears symmetrically opposite the first, causing their contributions to cancel and suppressing the thermoelectric response.

The Fig. 4(d) shows P_{MAX} with increasing ρ at fixed ω_{LC} . The extractable power increases with ρ , peaking near $\rho \simeq 1$, then decreases as multiphoton processes become dominant, distributing the bipolar thermoelectric capabilities on multiple channels. At higher T_j , the upper tail of the power distribution in ρ shrinks, reflecting the increased likelihood of multi-quanta energy exchange. Compared to the resistive configuration, the maximum extractable power is roughly an order of magnitude lower.

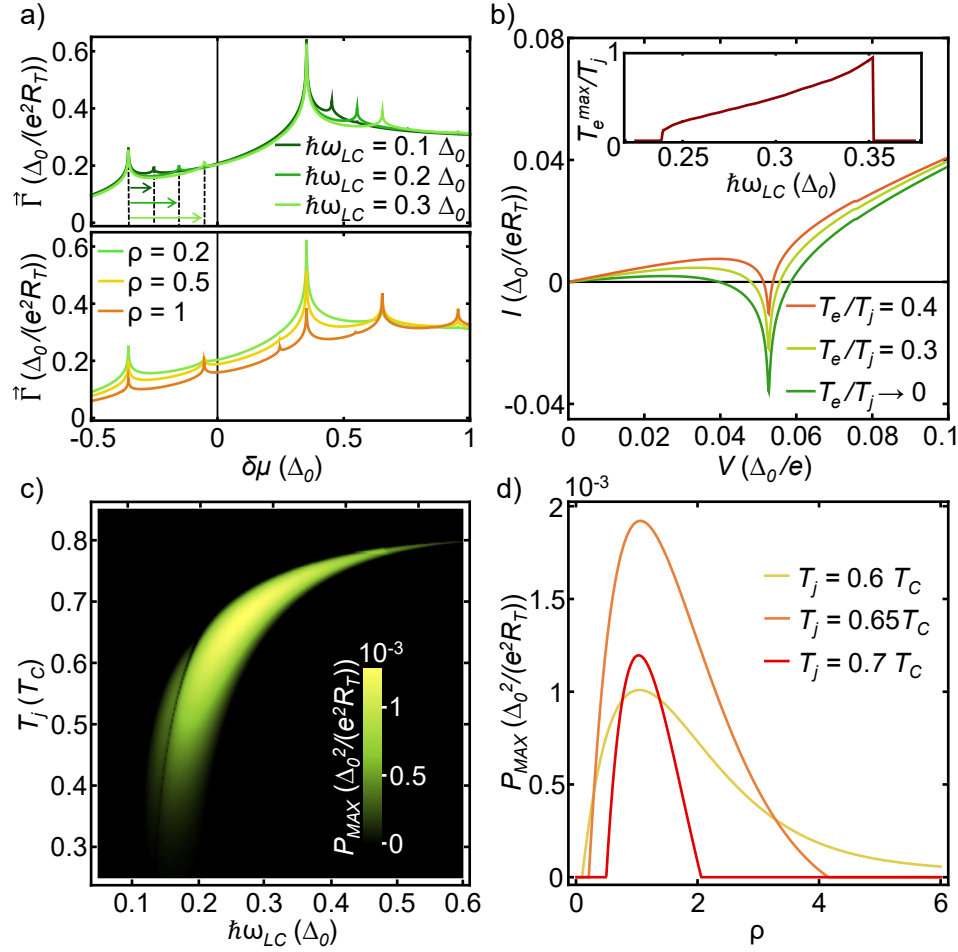


FIG. 4. (a) Top Panel: Forward tunneling rate $\bar{\Gamma}(\delta\mu)$ for three different environmental resonance frequencies, $\hbar\omega_{LC} = 0.1\Delta_0$ (dark green), $\hbar\omega_{LC} = 0.2\Delta_0$ (green), and $\hbar\omega_{LC} = 0.3\Delta_0$ (light green), with fixed parameters $T_e = 0$, $T_j = 0.7T_C$, $r = 0.8$, and $\rho = 0.2$. Bottom panel: $\bar{\Gamma}$ as a function of energy for fixed $\hbar\omega_{LC} = 0.3\Delta_0$ and varying coupling strengths: $\rho = 0.2$ (light green), $\rho = 0.5$ (yellow), and $\rho = 1$ (brown), with all other parameters unchanged. (b) I - V characteristic for three different environmental temperatures: $T_e = 0$ (green), $T_e = 0.3T_j$ (light green), and $T_e = 0.4T_j$ (red), with $T_j = 0.7T_C$, $r = 0.8$, $\hbar\omega_{LC} = 0.3\Delta_0$ and $\rho = 1$. Inset: maximum environmental temperature T_e^{MAX} allowing thermoelectric operation as a function of ω_{LC} for $T_j = 0.7T_C$ and $r = 0.8$. (c) Density plot of the extractable thermoelectric power at the peak (P_{MAX}) as a function of T_j and ω_{LC} , for $r = 0.8$ and $\rho = 0.5$. (d) P_{MAX} as a function of ρ , for three different junction temperatures: $T_j = 0.6T_C$ (yellow), $T_j = 0.65T_C$ (orange), and $T_j = 0.7T_C$ (red), with fixed resonance frequency $\hbar\omega_{LC} = 0.25\Delta_0$ and $r = 0.8$.

- [1] G.-L. Ingold and Y. V. Nazarov, Charge Tunneling Rates in Ultrasmall Junctions, in *Single Charge Tunneling: Coulomb Blockade Phenomena In Nanostructures*, edited by H. Grabert and M. H. Devoret (Springer US, Boston, MA, 1992), pp. 21–107.
- [2] Y. V. Nazarov and Y. M. Blanter, *Quantum Transport: Introduction to Nanoscience* (Cambridge University Press, 2009).
- [3] A. Hijano, F. Bergeret, F. Giazotto, and A. Braggio, Microwave-Assisted Thermoelectricity in S-I-S' Tunnel Junctions, *Phys. Rev. Appl.* **19**, 044024 (2023).
- [4] G. Germanese, F. Paolucci, G. Marchegiani, A. Braggio, and F. Giazotto, Bipolar thermoelectric Josephson engine, *Nat. Nanotechnol.* **17**, 1084 (2022).